PHOTONIC SENSORS / Vol. 7, No. 4, 2017: 372–376

A Micro S-Shaped Optical Fiber Temperature Sensor Based on Dislocation Fiber Splice

Haitao YAN[1,2*], Pengfei LI[1], Haojie ZHANG[2], Xiaoyue SHEN[2], and Yongzhen WANG[2]

[1]*College of Physics Engineering, Henan University of Science & Technology, Luoyang, 471003, China*

[2]*The Puyang Photoelectric Industry Technology Institute, Pu Yang, 457100, China*

[*]Corresponding author: Haitao YAN E-mail: yanhaitaoyht@163.com

Abstract: We fabricated a simple, compact, and stable temperature sensor based on an S-shaped dislocated optical fiber. The dislocation optical fiber has two splice points, and we obtained the optimal parameters based on the theory and our experiment, such as the dislocation amount and length of the dislocation optical fiber. According to the relationship between the temperature and the peak wavelength shift, the temperature of the environment can be obtained. Then, we made this fiber a micro bending as S-shape between the two dislocation points, and the S-shaped micro bending part could release stress with the change in temperature and reduce the effect of stress on the temperature measurement. This structure could solve the problem of sensor distortion caused by the cross response of temperature and stress. We measured the S-shaped dislocation fiber sensor and the dislocation fiber without S-shape under the same environment and conditions, and the S-shaped dislocation fiber had the advantages of the stable reliability and good linearity.

Keywords: Dislocated optical fiber; temperature sensor; interference; cross-sensitivity

Citation: Haitao YAN, Pengfei LI, Haojie ZHANG, Xiaoyue SHEN, and Yongzhen WANG, "A Micro S-Shaped Optical Fiber Temperature Sensor Based on Dislocation Fiber Splice," *Photonic Sensors*, 2017, 7(4): 372–376.

1. Introduction

Optical fiber sensors have the advantages of inexpensiveness, compactness, low weight, and immunity to electromagnetic interference, which results in a great demand for fiber sensors in the sensing applications. In all kinds of optical fiber sensors, temperature and stress sensors are the first to be developed [1]. Now, many optical methods and typical structures are used to research of temperature and stress fiber sensors, and the main methods include using Rayleigh scattering [2], Raman scattering [3], reflection [4], interference [5], evanescent field [6], and so on, and measuring optical signal intensity, phase, polarization state changes with the temperature or stress variation [7–8]. The mainly used optical structure has the Fabry-Perot (F-P) cavity [9], fiber grating [10], fiber grating array [11], and fiber ring resonator [12], and the applied fiber has a single-mode and multimode, photonic crystal fiber, microstructured fiber, and birefringent fiber. In above methods, the fiber Mach-Zehnder interference (MZI) has the advantages of simple structure, low cost, high sensitivity, and stability. Recently, some special structures were also proposed to fabricate the MZI, such as micromachining the fiber by femtosecond laser [13], splicing a section of single-mode

Received: 25 June 2017 / Revised: 19 July 2017

DOI: 10.1007/s13320-017-0450-0
Article type: Regular

noncircular twin-core fiber [14], splicing special double-cladding fiber [15] between standard single-mode fibers (SMFs), or splicing the fiber with dislocation [16]. However, fiber MZI-based sensors exhibited the cross-sensitivity between temperature and stress. It is also one of the key problems in the practical application of optical fiber sensors.

In our work, we demonstrated a simple, compact, and stable temperature MZI fiber sensor based on an S-shaped dislocated optical fiber. This sensor was fabricated by means of splicing a section of one standard SMF with two standard SMFs. And two splice points have a micro dislocation. Then this fiber was given a micro bending as S-shape, and the S-shaped micro bending part could release stress with the change in temperature. Several advantages are involved in the proposed sensor, such as high stability and linearity.

2. Sensor fabrication

As shown in Fig. 1(a), an amplified spontaneous emission (ASE) source with a laser wavelength ranging from 1530 nm to 1560 nm, an optical spectrum analyzer (OSA) (Ando AQ6317D2), and an optical circulator were employed to monitor the spectrum of the proposed based sensor, which was fabricated as described below.

Firstly, a section of the standard SMF (Corn G.652) with the core and cladding diameters of 9 μm and 125 μm, respectively was spliced to two standard SMFs, with a 2 μm – 10 μm offset between the two fiber cores by use of a commercial fusion splicer machine (Fujikura, FSM-100P+), in which there are two pairs of motors, i.e. the axial and vertical moving motors, with a movement accuracy of 0.01 μm and 0.1 μm, respectively.

As shown in Fig. 1(b), the light transmitting in SMF1 is divided into two parts at the misalignment-spliced joint. A part of light is coupled into the core of SMF2 as a core mode, and the other part of the light is coupled into the cladding of SMF2 as cladding modes. The two parts of the light will be coupled into the core of the lead-in SMF3. The two parts light of SMF2 formed the MZI in the SMF2 fiber, and an MZI-based sensor in one fiber was achieved. Then, as shown in Fig. 1(a), we measured the dislocation fiber MZI-based sensor.

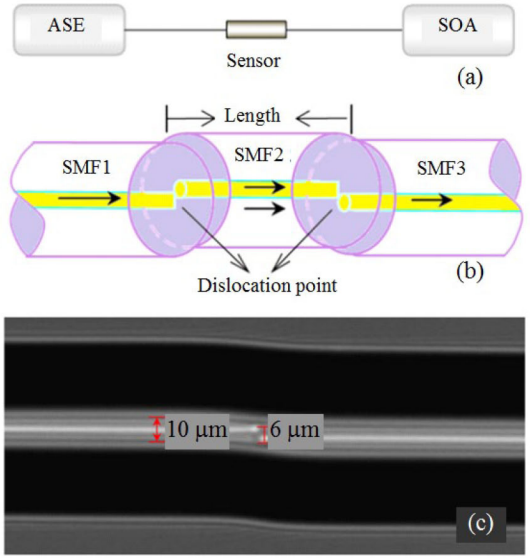

Fig. 1 Microscope image of the dislocation fiber: (a) schematic diagram of the proposed dislocation fiber MZI-based sensor measurement system, (b) schematic diagram of the dislocation fiber MZI-based sensor, and (c) microscope image of the point of dislocation fiber (6 μm).

In order to determine the offset and the length of SMF2, we measured the transmission of the sensor with different offsets and lengths of SMF2 under the temperature of 20 ℃, respectively. The results are shown in Figs. 2 and 3.

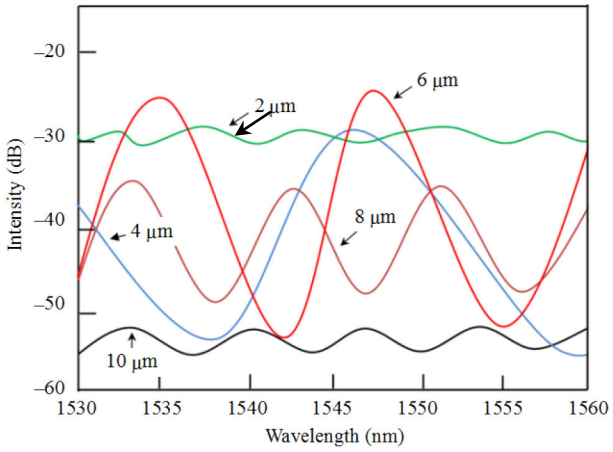

Fig. 2 Spectra of the dislocation fiber MZI-based sensor with offsets of 2 μm, 4 μm, 8 μm, 10 μm, and a SMF2 length of 6 mm, respectively.

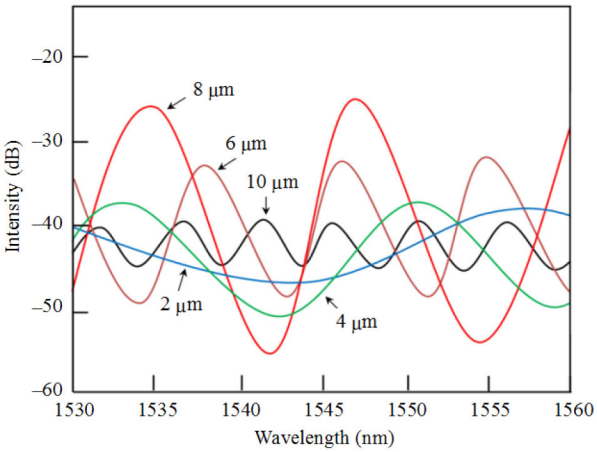

Fig. 3 Spectra of the dislocation fiber MZI-based sensor with SMF2 length of 2 mm, 4 mm, 6 mm, 8 mm, 10 mm, and offsets of 6 μm.

As shown in Fig. 2, the spectra of our sensor have the offsets of 2 μm, 4 μm, 6 μm, 8 μm, 10 μm, and an SMF2 length of 6 mm, respectively. Each sample sensor with a certain core offset exhibits a distinct fringe contrast in the interference patterns due to the core-offset-induced change in the ratio of lights coupled into the core and cladding modes in SMF2. And it can be found from Fig. 2 that the sample sensor with a core offset of 6 μm has the largest fringe contrast of 28.18 dB.

As shown in Fig. 3, the spectra of dislocation fiber MZI-based sensor have SMF2 lengths of 2 mm, 4 mm, 8 mm, 10 mm, and offsets of 6 μm. A clear interference fringes pattern is observed in those spectra. Each sample with different SMF2 lengths exhibits a distinct fringe contrast in the interference patterns. From Fig. 3, the sample sensor with an SMF2 length of 6 mm has the largest fringe contrast.

With the above results, the fringe has the largest fringe contrast when the offset of the sensor is 6 μm and the length of SMF2 is 6 mm. Moreover, we calculate the free spectrum range (FSR) of the interference fringes by

$$\Delta\lambda_{\text{dip}}^{m} \approx \frac{\lambda}{2\Delta n_{\text{eff}}^{m} L} \tag{1}$$

where $\Delta n_{\text{eff}}^{m}$ is the effective refractive index (RI) difference between the core and mth cladding modes in SMF2, and L is the length of SMF2. The measured FSR of the sensor with the offset 6 μm and the length of SMF2 6 mm is about 4.97 nm.

Based on the above parameters, the sensor with the offset 6 μm and the length of SMF2 6 mm was bended as S-shape and packaged. The part of dislocation fiber SMF1 and the SMF3 was inserted into the capillary steel tubes and fixed with epoxy resin glue. And then, the two capillary steel tubes were fixed on the micro displacement platform, a small displacement was given in the vertical direction, and the dislocation fiber SMF2 part became an S-shaped. As shown in Fig. 4, the packaged optical fiber was packaged with a package housing, protective sleeve, and some heat conducting oil to form a true temperature sensor.

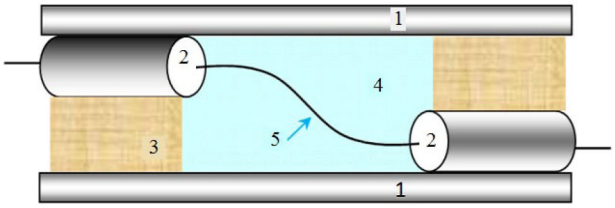

Fig. 4 Schematic diagram of the sensor with S-shaped bending and packaged (1: package housing; 2: capillary steel tube; 3: protective sleeve; 4: heat conducting oil; and 5: dislocation fiber).

3. Measurements and discussions

We tested the characteristics of the sensor in the case of temperature changes. The test method is in accordance with Fig. 1(a). The test results are shown in Fig. 5. The temperature range was 20 ℃ – 80 ℃, and the step size was 10 ℃. Obviously, we can see from the spectra that in the case of temperature change, the fringe retention and stability are very good. Taking the wave through near the 1545 nm wavelength as an example, the offset of the central wavelength is about 0.5 nm per –10 ℃. So we can obtain the temperature sensitivity $s=\Delta\lambda/\Delta T$ = 0.05 nm/℃ = 50 pm/℃. The results proved that our sensor was mainly temperature sensitive, avoiding the sensitive cross between the temperature and stress. The reasons are as follows.

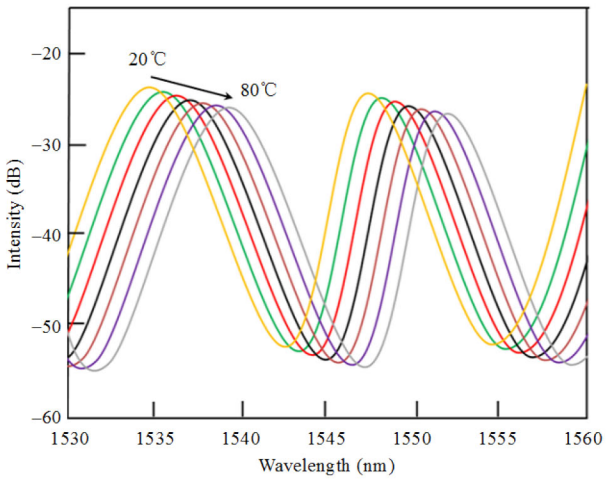

Fig. 5 Spectra evolution of the MZI-based sensor with different temperatures from 20 ℃ to 80 ℃, per–10℃ (polynomial fits).

The light propagating at the dislocation point between SMF1 and SMF2 was equally split into two beams in SMF2, which were propagating as the core mode and cladding mode. The two beams coupled into the core of SMF3 at the dislocation point between SMF2 and SMF3. We denote the intensities of the core mode and cladding mode in SMF2 as I_{co} and I_{cl}, and the output intensity of sensor can be expressed as

$$I = I_{co} + I_{cl} + 2\sqrt{I_{co} I_{cl}} \cos\left(\frac{2\pi l \Delta n}{\lambda} + \varphi_0\right) \quad (2)$$

where λ is the light wavelength, L is the length of SMF2, $\Delta n = n_{co} - n_{cl}$ is the effective RI difference between the two interference arms of MZI, where n_{co} and n_{cl} are the effective RIs of the core mode and the cladding mode, and the φ_0 is the initial phase of the interference. From (2), the interference spectrum reaches the minimum value when the following condition is satisfied:

$$\frac{2\pi l \Delta n}{\lambda_k} + \varphi_0 = (2k+1)\pi \quad (3)$$

where k is an integer, and λ_k is the wavelength of the kth order interference dip.

When the temperature changes, the sensor's maximum response is the length of SMF2. The change is due to the length of the interference arm. But, in the dislocation fusion point, the stress effect will lead to a lateral change. Therefore, the change in L with temperature is as

$$\Delta L = \mathrm{i}\Delta L_T + \mathrm{j}\Delta L_S \quad (4)$$

where ΔL_T is corresponding to the temperature changes, and ΔL_S is corresponding to the change in stress. So the interference fringe was a relationship between ΔL_T and ΔL_S.

We made the sensor in S-shape, which was given a stress with slow release in the process of temperature change. It counteracted the stress effect of ΔL_S. So, the offset was caused by temperature ΔL, which contains only a ΔL_T.

4. Conclusions

We demonstrated a temperature senor based on an S-shaped dislocated optical fiber. We made this fiber a micro bending as S-shape, and the S-shaped micro bending part could release stress with the change in temperature and reduce the effect of stress on the temperature measurement, and this structure solved the problem of sensor distortion caused by the cross response of temperature and stress. The senor has very good linear, retention, and stability, which can utilize the difference between the lengths of the dislocation points to achieve cascade and multipoint monitoring.

Acknowledgment

This work is sponsored by the the National Nature Science Foundation of China (No. 61675064), Henan Industrial Technology Innovation Program, and Puyang Major Scientific and Technological Project.

References

[1] I. W. Jung, B. Park, J. Provine, R. T. Howe, and O.

Solgaard, "Highly sensitive monolithic silicon photonic crystal fiber tip sensor for simultaneous measurement of refractive index and temperature," *Journal of Lightwave Technology*, 2011, 29(9): 1367–1374.

[2] D. X. Hua, M. Uchida, and T. Kobayashi, "Ultraviolet Rayleigh-Mie lidar with Mie-scattering correction by Fabry-Perot etalons for temperature profiling of the troposphere," *Applied Optics*, 2005, 44(7): 1305–1314.

[3] H. Y. Sun, S. C. Lien, Z. R. Qiu, H. C. Wang, T. Mei, C. W. Liu, *et al.*, "Temperature dependence of Raman scattering in bulk 4H-SiC with different carrier concentration," *Optics Express*, 2013, 21(22): 26475–26482.

[4] M. Kezmah and D. Donlagic, "All-fiber low-cost single-point and quasi-distributed evanescent field temperature sensors with extended temperature measurement range, based on standard telecommunication graded index fibers," *Applied Optics*, 2008, 47(23): 4212–4220.

[5] J. Roths, G. Andrejevic, R. Kuttler, and M. Süßer, "Calibration of fiber bragg cryogenic temperature sensors," *Optical Fiber Sensors*, 2006, 8383(3): 538–555.

[6] D. Donlagic and M. Lesic, "All-fiber quasi-distributed polarimetric temperature sensor," *Optics Express*, 2006, 14(22): 10245–10254.

[7] J. He, C. R. Liao, K. M. Yang, S. Liu, G. L. Yin, B. sun, *et al.*, "High-sensitivity temperature sensor based on a coated single-mode fiber loop," *Journal of Lightwave Technology*, 2015, 33(19): 4019–4026.

[8] A. Wang, G. Z. Wang, K. A. Murphy, and R. O. Claus, "Fiber-optic temperature sensors based on differential spectral transmittance/reflectivity and multiplexed sensing systems," *Applied Optics*, 1995, 34(13): 2295–2300.

[9] H. Zhang, Y. S. Qiu, Z. T. Huang, J. Z. Jiang, G. M. Li, H. X. Chen, *et al.*, "Temperature and vibration robustness of reflecting all-fiber current sensor using common single-mode fiber," *Journal of Lightwave Technology*, 2014, 32(22): 3709–3715.

[10] T. Stańczyk, K. Wysokiński, M. Filipowicz, T. Tenderenda, K. Gibała, H. Krisch, *et al.*, "Electrolytic joints between metal surfaces and metal-coated fibers for application in high temperature optical fiber sensors," *Journal of Lightwave Technology*, 2015, 33(12): 2480–2485.

[11] S. Rizzolo, E. Marin, A. Morana, A. Boukenter, Y. Ouerdane, M. Cannas, *et al.*, "Investigation of coating impact on OFDR optical remote fiber-based sensors performances for their integration in high temperature and radiation environments," *Journal of Lightwave Technology*, 2016, 34(19): 4460–4465.

[12] E. R. Vera, C. M. B. Cordeiro, and P. Torres, "Highly sensitive temperature sensor using a Sagnac loop interferometer based on a side-hole photonic crystal fiber filled with metal," *Applied Optics*, 2017, 56(2): 156–162.

[13] G. Liu, M. Han, and W. Hou, "High-resolution and fast-response fiber-optic temperature sensor using silicon Fabry-Pérot cavity," *Optics Express*, 2015, 23(6): 7237–7247.

[14] S. J. Weng, L. Pei, J. S. Wang, T. G. Ning, and J. Li, "High sensitivity d-shaped hole fiber temperature sensor based on surface plasmon resonance with liquid filling," *Photonics Research*, 2017, 5(2): 103–107.

[15] W. J. Yoo, K. W. Jang, J. K. Seo, J. Y. Heo, J. S. Moon, J. Y. Park, *et al.*, "Development of respiration sensors using plastic optical fiber for respiratory monitoring inside MRI system," *Journal of the Optical Society of Korea*, 2010, 14(3): 235–239.

[16] B. Dong, D. P. Zhou, and L. Wei, "Temperature insensitive all-fiber compact polarization-maintaining photonic crystal fiber based interferometer and its applications in fiber sensors," *Journal of Lightwave Technology*, 2101, 28(7): 1011–1015.